JACS
JOURNAL OF THE AMERICAN CHEMICAL SOCIETY

Article

pubs.acs.org/JACS

Role of Nanomechanics in Canonical and Noncanonical Pro-angiogenic Ligand/VEGF Receptor-2 Activation

Daniele Maiolo,[†,‡,∥] Stefania Mitola,[‡,∥] Daria Leali,[‡] Giulio Oliviero,[†] Cosetta Ravelli,[‡] Antonella Bugatti,[‡] Laura E. Depero,[†] Marco Presta,*[,‡] and Paolo Bergese*[,†]

[†]Chemistry for Technologies Laboratory and INSTM, School of Engineering, University of Brescia, Via Branze, 38, 25123 Brescia, Italy

[‡]Unit of General Pathology, Department of Biomedical Sciences and Biotechnology, School of Medicine, University of Brescia, Viale Europa 11, 25123, Brescia, Italy

Supporting Information

ABSTRACT: Vascular endothelial growth factor receptor-2 (VEGFR2) is an endothelial cell receptor that plays a pivotal role in physiologic and pathologic angiogenesis and is a therapeutic target for angiogenesis-dependent diseases, including cancer. By leveraging on a dedicated nanomechanical biosensor, we investigated the nanoscale mechanical phenomena intertwined with VEGFR2 surface recognition by its prototypic ligand VEGF-A and its noncanonical ligand gremlin. We found that the two ligands bind the immobilized extracellular domain of VEGFR2 (sVEGFR2) with comparable binding affinity. Nevertheless, they interact with sVEGFR2 with different binding kinetics and drive different in-plane piconewton intermolecular forces, suggesting that the binding of VEGF-A or gremlin induces different conformational changes in sVEGFR2. These behaviors can be effectively described in terms of a different "nanomechanical affinity" of the two ligands for sVEGFR2, about 16-fold higher for VEGF-A with respect to gremlin. Such nanomechanical differences affect the biological activity driven by the two angiogenic factors in endothelial cells, as evidenced by a more rapid VEGFR2 clustering and a more potent mitogenic response triggered by VEGF-A in respect to gremlin. Together, these data point to surface intermolecular interactions on cell membrane between activated receptors as a key modulator of the intracellular signaling cascade.

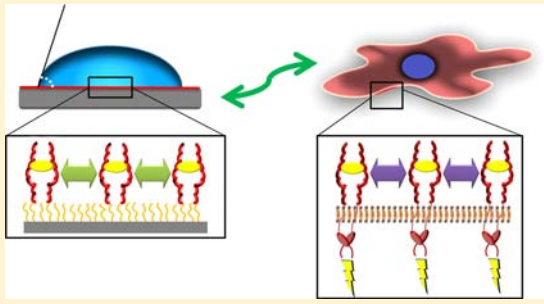

INTRODUCTION

Cell signaling, the set of intracellular events that translate extracellular information to adaptive intracellular responses, is triggered by the modulation between ligand−receptor recognition and membrane nanomechanical events, including conformational changes and clustering of the activated receptors[1] (Figure 1), according to mechanisms that are still largely elusive.[2−6] Advancing this understanding has important implications both in basic science and in translational medicine when considering that ligand−receptor recognition represents a therapeutic target toward drug development in various human diseases.

Cell membrane growth factor receptors play an important role in different physiological and pathological processes, including cancer.[7] In particular, the dependence of solid tumors on the formation of a novel vessel network for growth, survival, and metastatic dissemination (a process named "tumor angiogenesis") makes the pro-angiogenic molecular machinery a target for new interventions in cancer therapy.[8,9] This strategy requires a deep understanding of the interactions of pro-angiogenic growth factors with their cognate cell membrane tyrosine kinase receptors that lead to a complex array of transduction signals in activated endothelium.[10]

Nanomechanical biosensors[11] feature the inherent ability to translate protein surface conformational changes and in-plane interactions into a macroscopic surface mechanical work.[12,13] They probe with high fidelity the fact that part of the free energy released by a ligand−receptor surface recognition is spent to "accommodate" the ligands on the surface and to drive other molecular rearrangements such as ligand conformational changes and clustering or solvent and electrolyte displacement (Figure 1).[14] All of these phenomena ultimately trigger a variation of the in-plane intermolecular forces, which macroscopically accumulate in a surface tension that can range from few to several tens of mJ/m^2 (mN/m), and thus can be probed by nanoliter CONtact Angle MOlecular REcognition (CONAMORE, Figure 3a)[15,16] or other mechanical biosensors, such as microcantilever (MC) beams.[17,18] Nevertheless, despite these potential implications, nanomechanical biosensors have not been effectively deployed to investigate pro-angiogenic ligand−receptor interactions.

In view of this, we assessed CONAMORE to investigate key ligand interactions of the vascular endothelial growth factor (VEGF) receptor-2 (VEGFR2), which is the major pro-

Received: June 15, 2012
Published: August 3, 2012

   dx.doi.org/10.1021/ja305816p | J. Am. Chem. Soc. 2012, 134, 14573−14579

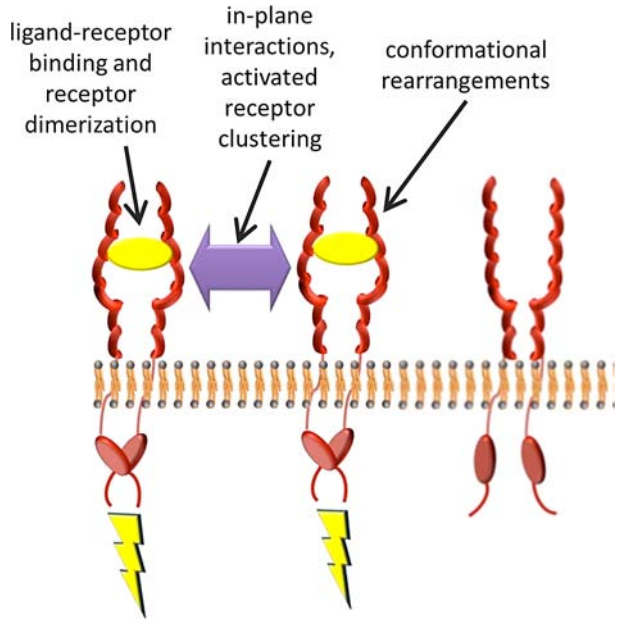

Figure 1. Cell membrane ligand–receptor nanomachinery. The cartoon depicts the nanoscale surface mechanisms developed on cell membrane by ligand–receptor recognition, including ligand–receptor binding, in-plane intermolecular interactions, and conformational rearrangements of the receptor. Activation of this nanomachinery triggers intracellular signaling and biological responses.

angiogenic receptor expressed by endothelial cells.[19] VEGFR2 plays critical functions in physiological and pathological angiogenesis through distinct signal transduction pathways regulating endothelial cell survival, proliferation, migration, vascular permeability, tubulogenesis, and gene expression.[20] VEGFR2 is activated by different members of the VEGF family, including the major pro-angiogenic factor VEGF-A. These ligands show different receptor activation abilities,[21,22] suggesting a role of molecular surface nanomachinery in triggering intracellular signaling events.[23,24] Also, recent observations from our laboratory have identified the bone morphogenic protein-antagonist gremlin as a novel pro-angiogenic ligand of VEGFR2, distinct from canonical VEGFs, increasing the complexity of extracellular interactions involving this receptor.[25]

Here, we quantified the in-plane forces developed upon surface recognition of VEGFR2 by the prototypic ligand VEGF-A and the noncanonical ligand gremlin. To this purpose, we probed the interactions of the extracellular domain of VEGFR2 (sVEGFR2) with these ligands by integrating surface plasmon resonance (SPR) spectroscopy[26] data with nanoliter CONAMORE assays. We found that different in-plane intermolecular attractive interactions arise along with VEGF-A/sVEGFR2 and gremlin/sVEGFR2 recognition and quantified them. These differences are mirrored by differences in the modulation of the biological processes subtending VEGFR2 engagement by the two pro-angiogenic factors in endothelial cells, as shown by in vivo fluorescence resonance energy transfer (FRET) analysis of receptor activation[27] and cell proliferation assays.

RESULTS AND DISCUSSION

Binding Affinity. VEGF-A/sVEGFR2 and gremlin/sVEGFR2 surface recognition were first characterized by SPR spectroscopy as described in refs 25 and 28. SPR features a label-free mass detection by measuring the variation of the refractive index at the solid–solution interface upon the capture of the ligand by the surface immobilized receptor.[29]

To this purpose, recombinant human sVEGFR2 was immobilized onto Au-coated SiO_2 chips derivatized with a 100 nm thick dextran layer, and binding of increasing nanomolar concentrations of VEGF-A or gremlin was tracked as a function of time by SPR intensity change, here expressed as response units (RU). For each concentration of the ligand, the SPR response at equilibrium was used to build the dose–response normalized binding isotherms shown in Figure 2 (see

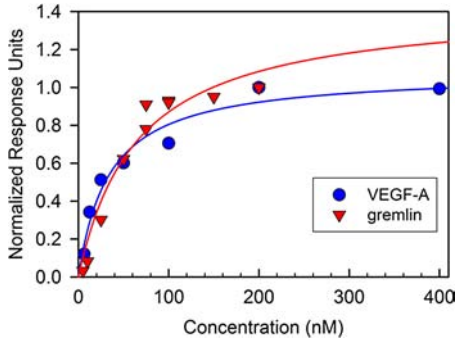

Figure 2. Normalized SPR binding isotherms of VEGF-A (blue circle) and gremlin (red triangle) with sVEGFR2 immobilized on a 100 nm dextran-coated gold surface. Data points represent the normalized mean SPR signal of two replicate experiments. The continuous lines are the Langmuir fits for the data points.

the Experimental Section for further details). The SPR isotherms of VEGF-A and gremlin substantially overlap, demonstrating that a similar number of VEGF-A and gremlin molecules interact with sVEGFR2 (i.e., VEGF-A and gremlin have similar extent of binding). This is confirmed by the values of the surface mass dissociation constants, K_d^σ mass, determined by fitting the SPR data to the Langmuir equation for monovalent binding, that are equal to K_d^σ mass = (34 ± 8) nM and K_d^σ mass = (65 ± 20) nM for VEGF-A and gremlin, respectively.

It must be pointed out that we termed the dissociation constant obtained by SPR as "surface mass dissociation constant" to underline that (i) this thermodynamic parameter relies on quantification of surface-bound mass and may substantially differ from the one evaluated in ideal solution,[30] and (ii) to distinguish it from the "surface nanomechanical affinity" (see below).

Despite similar K_d^σ mass values, SPR analysis revealed substantial differences between VEGF-A/sVEGFR2 and gremlin/sVEGFR2 interactions in terms of binding and dissociation kinetic rate constants, k_{on} and k_{off} (evaluation details in the Experimental Section). As reported in Table 1, even though the binding of the two ligands to sVEGFR2 occurs at the same rate, the dissociation of VEGF-A from the receptor complex is about 10-fold slower than for gremlin. This may be ascribed to different surface nanomechanical phenomena occurring along with the recognition of the two ligands. In particular, the data point to the possibility that VEGFR2 adopts different conformations after binding with VEGF-A or gremlin, mirrored by different release rates of the two ligands.[31] Similar packing related kinetics have been recently observed by Duyne and co-workers.[32]

dx.doi.org/10.1021/ja305816p | J. Am. Chem. Soc. 2012, 134, 14573–14579

Table 1. Mass and Mechanical VEGF-A/sVEGFR2 and Gremlin/sVEGFR2 Binding Parameters Evaluated by SPR and CONAMORE[a]

	k_{on} (M^{-1} s^{-1})	K_{off} (s^{-1})	K_d^σ mass (nM)	K_d^σ mech (nM)
VEGF-A	$(8.5 \pm 3) \times 10^4$	$(1.5 \pm 0.3) \times 10^{-4}$	34 ± 8	2 ± 0.7
gremlin	$(8 \pm 2) \times 10^4$	$(2 \pm 0.3) \times 10^{-3}$	65 ± 20	32 ± 9

[a] k_{on} and k_{off}: Binding and dissociation kinetic rate constants, respectively. K_d^σ mass: Surface mass dissociation constant. K_d^σ mech: Surface nanomechanical dissociation constant.

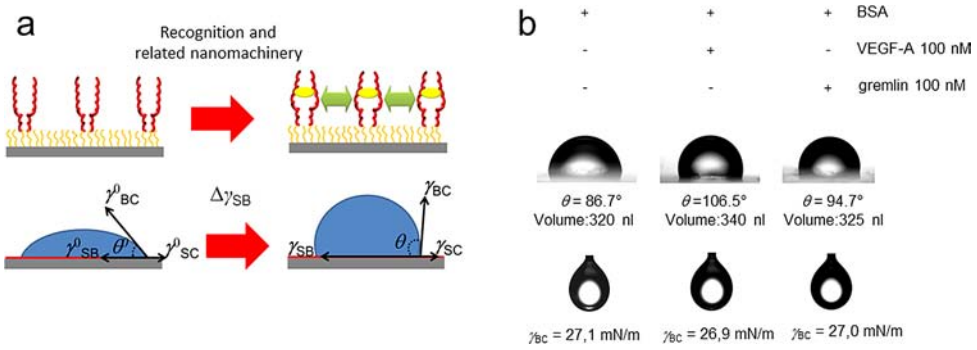

Figure 3. CONAMORE (CONtact Angle MOlecular REcognition) analysis of ligand–sVEGFR2 interaction. (a) The nanomachinery occurring on sVEGFR2-immobilized chip following ligand recognition (top scheme) triggers a variation of the interfacial tension $\Delta\gamma_{SB}$ that can be quantified by sessile drop contact angle experiments (bottom scheme). For the description of the other scheme parameters, see the main text. (b) (top) Representative nanoliter sessile droplets of reference (BSA) and ligand (VEGF-A or gremlin) solutions deposited onto a sVEGFR2 chip and (bottom) of the respective pendant drops; all drops are in cyclohexane surrounding phase. The images were digitally analyzed to evaluate the contact angle, θ, and the solution–cyclohexane interfacial tension, γ_{BC}.

Nanomechanical Affinity. To assess the nanomechanical phenomena related to ligand–VEGFR2 surface recognition, we used CONAMORE. Among the available nanomechanical biosensors, CONAMORE best suited our needs, as it could be performed on the same chips used for SPR experiments, offering the best conditions for data comparison, and requires 10–100-fold less solution of ligand for each experiment (e.g., few microliters vs hundreds of microliters) with respect to commercial MC platforms.[16]

CONAMORE is based on the sessile drop contact angle principle. When a droplet is placed onto a solid surface, it reaches equilibrium with the surface and the surroundings under the action of the interfacial tensions at the contact line at which drop, surface, and surroundings meet, forming a definite contact angle.[33] The way this familiar phenomenon was exploited to probe surface nanomechanics of ligand/sVEGFR2 recognition is sketched in Figure 3a. Here, the surface, phase S, is the sVEGFR2-functionalized chip; the droplet, phase B, is a 1 μM BSA solution in phosphate buffered saline at pH 7.4 (hereafter referred as BSA solution) added or not with the ligand under test; and the surrounding phase C is cyclohexane. The ligand/sVEGFR2 recognition makes a specific contribution to the solid–solution interfacial tension, γ_{SB}, that is missed in the interfacial tension of the reference system γ^0_{SB}. Recognition is thus univocally associated with the differential of the solid–solution interfacial tensions of the two systems, $\Delta\gamma_{SB} = \gamma_{SB} - \gamma^0_{SB}$, that can be expressed as a function of the contact angles:[15]

$$\Delta\gamma_{SB} = \gamma_{SB} - \gamma^0_{SB} = \gamma^0_{BC}\cos\theta^0 - \gamma_{BC}\cos\theta \quad (1)$$

where θ^0 and θ are the contact angles of the reference and of the recognition systems, respectively, and γ^0_{BC} and γ_{BC} are the solution-surrounding phase interfacial tensions of the reference and of the recognition systems, respectively (Figure 3a). For further details about the theoretical foundations and biosensing applications of CONAMORE, see refs 14–16.

On this basis, the dose–response experiments performed with SPR were repeated with CONAMORE. Typical binding isotherms obtained by plotting $\Delta\gamma_{SB}$ as a function of ligand concentration are reported in Figure 4a. In view of the SPR

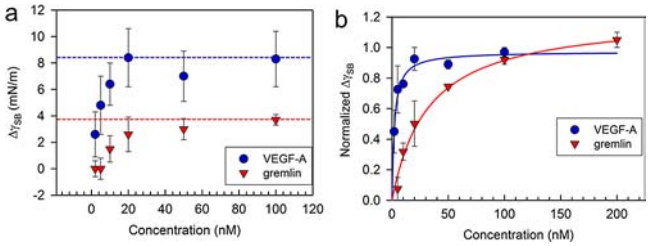

Figure 4. Nanomechanical study of the binding of VEGF-A and gremlin to surface immobilized sVEGFR2. (a) Representative $\Delta\gamma_{SB}$ binding isotherms of VEGF-A (blue ●) and gremlin (red ▼) with sVEGFR2 immobilized onto a 100 nm dextran-coated gold surface obtained by CONAMORE. The differential solid–solution interfacial tension, $\Delta\gamma_{SB}$, is referred to the BSA solution. Data points are the mean of three droplets deposited on the same chip; the error bars represent the SD of the mean. (b) Normalized $\Delta\gamma_{SB}$ binding isotherms (same legend as in the previous caption). Data points are the overall mean of two replicate experiments conducted on different chips; the error bars represent the SD of the mean.

data, the extent of binding of VEGF-A and gremlin match at any concentration. Therefore, the isotherms indicate that for the same extent of binding to surface-immobilized sVEGFR2, VEGF-A exerts a $\Delta\gamma_{SB}$ (blue ●) that is 2–5-fold higher than the $\Delta\gamma_{SB}$ exerted by gremlin (red ▼). At 100 nM, $\Delta\gamma_{SB}$ is 8.3 ± 2.1 and 3.7 ± 0.4 mN/m for VEGF-A and gremlin, respectively. Remarkably, these values are consistent with MC measurements of cooperative surface mechanical work performed by protein conformational changes.[12,13]

dx.doi.org/10.1021/ja305816p | J. Am. Chem. Soc. 2012, 134, 14573–14579

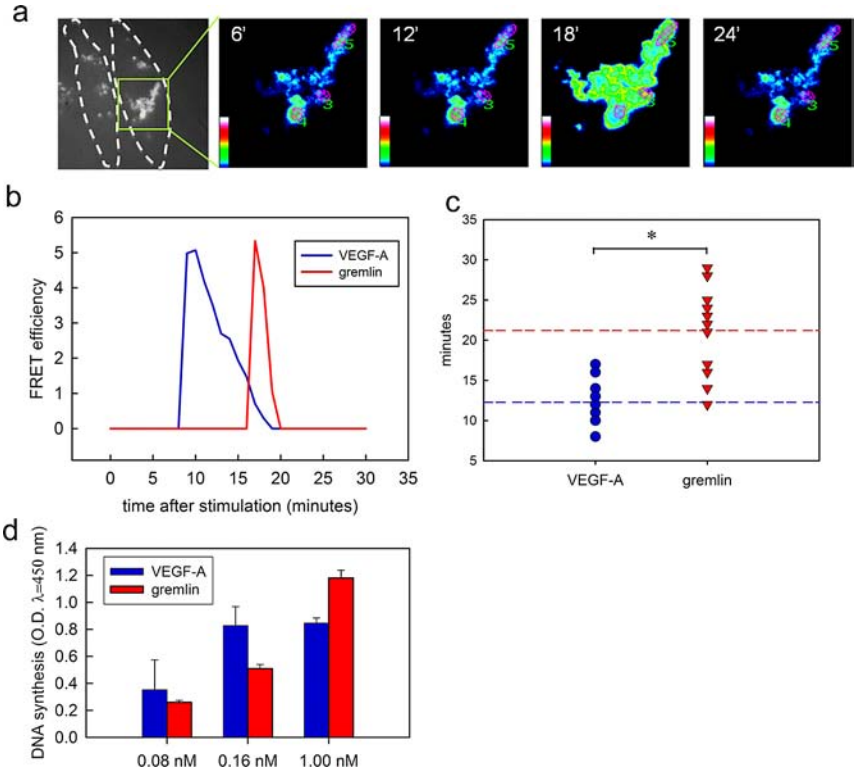

Figure 5. Biological processes following VEGFR2 engagement by VEGF-A and gremlin in endothelial cells. (a) BAECs were transiently cotransfected with the FRET pair VEGFR2-EYFP and VEGFR2-ECFP. After 48 h, 30 cells with similar expression of ECFP and EYFP proteins were analyzed for 10 min before and 30 min after stimulation with 1.2 nM VEGF-A or 2.0 nM gremlin. The sequence of the panels refers to intracellular FRET signal at different times in a selected zone of the region of interest (ROI) of the gremlin-stimulated cell evidenced by the white dotted line. FRET signal intensity is by the color scale, scoring for FRET levels from 0 (dark blue) to 10 (white). (b) Typical kinetics of intracellular FRET events versus time after ligand stimulation. FRET signals are quantified in the ROI after subtraction of FRET background signal (cell before ligand stimulation). (c) Time of appearance of FRET events in VEGF-A and gremlin stimulated cells. Each point represents one cell. (d) Serum-starved HUVECs were stimulated for 24 h with the indicated concentrations of VEGF-A (blue bars) or gremlin (red bars) and added with BrdU for 8 h. At the end of incubation, the levels of DNA incorporated BrdU were measured by ELISA.

No receptor interactions were observed when VEGF-A or gremlin were passed on 6.0 M urea unfolded sVEGFR2 or on dextran derivatized chips (Supporting Information). The specificity of interaction was further confirmed using TGF-β, a structural analogous of VEGF-A, which does not bind immobilized sVEGFR2 (Supporting Information).[34,35] These results, together with previous observations about the ability of neutralizing anti-VEGF-A antibodies to fully suppress sVEGFR2 interaction,[16] fully rule out any possible contribution of nonspecific binding events to $\Delta\gamma_{SB}$.

A deeper analysis of the nanomechanical information can be gained by considering the normalized $\Delta\gamma_{SB}$ dose−response isotherms and the related fits reported in Figure 4b. Comparison with the mass isotherms of Figure 2 suggests that the extent of binding and the nanomechanical response are not linearly proportional (a plot of $\Delta\gamma_{SB}$ vs extent of binding is provided in Supporting Information Figure S3), with the nanomechanical response saturating before the extent of binding. The deviation from linearity is more pronounced for VEGF-A, which drives the higher $\Delta\gamma_{SB}$. Similar behaviors have been recently observed for cocaine−aptamer complexes.[36]

By fitting the normalized $\Delta\gamma_{SB}$ isotherms to a Langmuir-like equation for monovalent binding, it is possible to extrapolate an apparent equilibrium constant that embraces the nanomechanical aspects of ligand/sVEGFR2 surface recognition. We name this thermodynamic parameter "surface nanomechanical affinity", K^{σ} mech, and its reciprocal, K_d^{σ} mech = $1/(K^{\sigma}$ mech), "surface nanomechanical dissociation constant". The VEGF-A isotherm displays a sharply steeper rise with respect to the gremlin one, indicating a significant difference in terms of K_d^{σ} mech. This is supported by the fitting results, which give K_d^{σ} mech = (2.0 ± 0.7) nM and K_d^{σ} mech = (32 ± 9) nM, for VEGF-A and gremlin, respectively. Thus, VEGF-A has about 16-fold higher surface nanomechanical affinity for sVEGFR2 with respect to gremlin, while they both present comparable extent of binding, that is, K_d^{σ} mass (see Table 1 for a summary of the binding parameters).

A further analysis of $\Delta\gamma_{SB}$ may provide molecular insight about the mechanisms of interaction of VEGF-A and gremlin with VEGFR2. Indeed, binding of both ligands to the immobilized receptor results in positive $\Delta\gamma_{SB}$ values, indicating that the mechanical surface work is tensile with respect to the solid surface (assuming the Gibbs dividing surface to be located within the dextran layer[37]), which implies that the in-plane interprotein forces are attractive for both VEGF-A/sVEGFR2 and gremlin/sVEGFR2 interactions. By taking into account that the surface density of the immobilized sVEGFR2 is (1.26 ± 0.03) × 10^{10} molecule/mm^2 (as evaluated by SPR, Supporting Information), we learn that each sVEGFR2 molecule occupies an area of ∼100 nm^2, matching the size of the VEGF-A/sVEGFR2 complex.[24] These data indicate we are reasonably dealing with a monolayer of sVEGFR2 and that the variation of the distance between sVEGFR2 molecules before and after ligand interaction spans from tenths to few nanometers. The

dx.doi.org/10.1021/ja305816p | J. Am. Chem. Soc. 2012, 134, 14573−14579

intermolecular force triggered by the complex formation can be estimated by multiplying the intermolecular distance change by $\Delta\gamma_{SB}$. For instance, a 0.5 nm change for the VEGF-A/sVEGFR2 complex with $\Delta\gamma_{SB}$ = 8.6 ± 0.7 mN/m results in a force of 4.3 ± 0.4 pN, consistent with the forces necessary to cause conformational changes in biomolecules.[38] These results suggest conformational rearrangements as the nanomechanical mechanism that modulates the in-plane interactions driving $\Delta\gamma_{SB}$, in agreement with the indications from binding kinetics.

Biological Response. Taken together, in vitro CONAMORE experiments evidence a significantly more intense in-plane attraction between VEGF-A/sVEGFR2 with respect to gremlin/sVEGFR2 complexes, suggesting possible differences in the in vivo biological responses exerted by the two pro-angiogenic factors on VEGFR2-expressing endothelium.[25]

Upon agonist interaction, activated VEGFR2 dimerizes and undergoes internalization within the early endosomal compartment of endothelial cells.[39] On this basis, to assess possible differences in the modulation of the biological processes subtending VEGFR2 engagement by the two pro-angiogenic factors, we performed in vivo FRET analysis of VEGF-A and gremlin-stimulated bovine aortic endothelial cells (BAECs) cotransfected with EYFP- and ECFP-tagged VEGFR2.[25] Even though both agonists promoted VEGFR2 clustering in ∼50% of treated BAECs, different kinetics of appearance of FRET events were obtained in VEGF-A versus gremlin stimulated cells. Indeed, VEGF-A leads to a more rapid receptor clusterization with respect to gremlin, the averaged time of appearance of FRET signals occurring 12.27 ± 2.93 and 21.18 ± 5.14 min after stimulation with the two agonists, respectively (Figure 5a–c). Next, we compared the ability of the two angiogenic factors to trigger DNA synthesis in endothelial cells. As shown in Figure 5d, VEGF-A and gremlin induced a maximum increase of DNA synthesis in serum-starved human umbilical vein endothelial cells (HUVECs) at 0.16 and 1.0 nM, respectively. Similar differences in biological activity were observed when HUVECs were tested for their capacity to migrate in response to increasing concentrations of VEGF-A or gremlin in a Boyden chamber assay.[25]

Although we cannot rule out a possible distinct role of cell membrane coreceptors in VEGFR2 activation by the two ligands, the differences observed in vivo between the prototypic ligand VEGF-A and the noncanonical agonist gremlin in time and dose-dependent VEGFR2 activation appear to reflect the quantified differences in nanomechanical affinity.

■ CONCLUSIONS

Our results indicate that surface in-plane receptor interactions driven by ligand–VEGFR2 recognition play a key role in modulation of VEGFR2-mediated cellular responses. We achieved this by implementing an investigation strategy that leverages on in vitro novel nanomechanical nanoliter CONAMORE biosensing, supported and integrated by SPR analysis, and in vivo FRET and cell proliferation experiments.

We found that VEGF-A and gremlin bind the extracellular domain of VEGFR2 with comparable binding affinity, but following different kinetics and driving up to 5-fold different in-plane intermolecular forces, which vary from few to several piconewton, suggesting that the binding of VEGF-A or gremlin induces different conformational changes in VEGFR2. To macroscopically quantify this phenomenon, we introduced the "surface nanomechanical affinity", which resulted about 16-fold higher for VEGF-A with respect to gremlin (0.50 ± 0.17 and 0.031 ± 0.008 nM^{-1}, respectively). Such nanomechanical differences affect the VEGFR2-dependent biological activity driven in vivo by the two pro-angiogenic factors in endothelial cells, as evidenced by a more rapid receptor clustering and a more potent biological response triggered by VEGF-A with respect to gremlin.

These findings strengthen the understanding of the role of ligand–receptor nanomachinery in regulating cell signaling and pave the way for its future systematic investigation, with an impact in molecular medicine and cell biology fields. For example, they suggest we may need a shift in perspective in drug screening models[40] by including molecular recognition nanomechanics. Or, on a longer term perspective, they propose a route toward one of the milestones fixed for bottom-up synthetic biology, identified in the characterization of the interactions between hybrid systems of nucleic acids, lipids, and proteins under well-defined conditions.[41]

■ EXPERIMENTAL SECTION

Biomolecules and Other Chemicals. sVEGFR2 was obtained from RELIATech GmbH (Braunschweig, Germany). Human recombinant VEGF-A_{165} and mouse recombinant gremlin were from R&D Systems (Minneapolis, MN). Suppliers of the other chemicals are given below.

Surface Plasmon Resonance (SPR) Spectroscopy. SPR experiments and analysis were performed following well-established procedures[42] that we recently assessed for the investigation of growth factors.[25,28] They were performed on a BIAcore X (BIAcore Inc., Piscataway, NJ).

sVEGFR2 was immobilized with a density of approximately (2.2 ± 0.03) × 10^{10} molecule/mm^2 to an Au-coated SiO_2 5 × 5 mm^2 chip derivatized with a 100 nm thick dextran layer (CMD50L, XanTec bioanalytics GmbH, Dusseldorf, Germany; see the Supporting Information for details on the SPR evaluation of the sVEGFR2 surface density). The chip was preactivated with a mixture of 0.2 M *N*-ethyl-*N*′-(3-dimethylaminopropyl)-carbodiimide hydrochloride and 0.05 M *N*-hydroxysuccinimide (35 μL; flow rate: 10 μL/min). After sVEGFR2/Fc immobilization (70 μL of a solution of 0.187 μM sVEGFR2/Fc in 10 mM sodium acetate pH 3 at flow rate: 10 μL/min), the remaining dextran active moieties were deactivated with 1.0 M ethanolamine at pH 8.5 (35 μL, flow rate 10 μL/min). The activated/deactivated dextran was used as a reference (control) system.

Binding of VEGF-A and gremlin to immobilized sVEGFR2 was monitored as a function of time by tracking the SPR intensity change upon binding progression. VEGF-A was scanned for concentrations ranging from 2.5 to 400 nM; gremlin was scanned for concentrations ranging from 5 to 200 nM. Both of the ligands were dissolved in HBS-EP buffer (0.01 M Hepes, pH 7.4 plus 0.005% surfactant P20, 0.15 M NaCl, 3 mM EDTA). The ligand solutions were flowed on the functionalized chip for 4 min. VEGF-A: sample volume 40 μL, flow rate 10 μL/min, and dissociation time 120 s. Gremlin: sample volume 40 μL, flow rate 5 μL/min, and dissociation time 240 s. Samples of the binding curves after subtraction of the reference signal are reported in Supporting Information Figure S1. The equilibrium (plateau) values of the sensorgrams were used to build the binding isotherms reported in Figure 3a, where the data points represent the normalized mean signal of two replicate experiments. Binding isotherm points were fitted to the Langmuir equation for monovalent binding,[43] and mass surface dissociation constant K_d^a mass and the scaling parameter Q_{max} were determined. The errors on these parameters were assigned as a result of the fitting algorithm (95% confidence bounds).

The binding and dissociation kinetic rate constants, k_{on} and k_{off}, were evaluated from fitting dose sensorgrams with a 1:1 Langmuir association/dissociation equation.[44] The k_{on} and k_{off} values reported in Table 1 represent the mean over a set of sensorgrams of the same ligand at different doses. The SD of the mean was taken as the error

(see Supporting Information Figure S1 and its caption for more details).

CONAMORE Experiments and Data Analysis. The experiments were implemented from the procedures we set in our previous work on CONAMORE analysis of interactions between growth factors.[16] CONAMORE chips were prepared analogously to the ones prepared for SPR, but without the assistance of microfluidics. To this purpose, as-received CMD50L chips were rinsed with HBS-EP buffer and activated by immersion for 3 h in 0.2 M *N*-ethyl-*N*-(3-dimethylaminopropyl)-carbodiimide hydrochloride plus 0.05 M *N*-hydroxysuccinimide. The surfaces were then washed with HBS-EP and incubated with 30 μL of sVEGFR2 1.87 μM in 10 mM sodium acetate pH 3.0 for 2 h at 25 °C and then for 14 h at 4 °C. After sVEGFR2 immobilization, preactivated matrix was neutralized with 1.0 M ethanolamine (pH 8.5). Finally, after an accurate HBS-EP wash, the functionalized chips were immersed in 10 mM NaOH for a few seconds, washed with HBS-EP, and stored in a phosphate saline buffered solution at pH 7.4 (PBS) at 4 °C. sVEGFR2 resulted immobilized on the chips with a density of approximately $(1.26 \pm 0.03) \times 10^{10}$ molecule/mm^2 (as evaluated by SPR, see the Supporting Information).

Ligands were dissolved in a 1 μM solution of BSA in phosphate saline buffered solution at pH 7.4 (BSA solution) that was left to pre-equilibrate with cyclohexane (the surrounding phase) overnight (to avoid solute exchange between the two phases during the experiments) and prefiltered before the ligand addition. The BSA solution was also employed as reference.

Sessile drop measurements were carried out at room temperature with a CAM 200 tensiometer (KSV Instruments, Finland) equipped with a Navitar camera following the protocols described in ref 16. The mean θ for each solution droplet was evaluated by three independent replicates deposited in three different zones of the same chip, and the SD of the mean was taken as the error. Before a sessile drop experiment was performed with a new solution, the chip was regenerated by a quick immersion in 10 mM NaOH (to remove the bound proteins) and sequential washings with PBS and Milli-Q water. Sessile drop experiments for each solution were confirmed by replicating them two times on two different chips.

Fitting of normalized $\Delta\gamma_{SB}$ binding isotherms reported in Figure 4b was conducted analogously to those of normalized SPR binding isotherms reported in Figure 2.

Determination of solution−cyclohexane interfacial tension, γ_{BC}, was performed through the standard pendant drop method.[37] The pendant drop images (Figure 3b) were analyzed by the Young−Laplace equation (KSV CAM Optical Contact Angle and Pendent Drop Surface Tension Software 4.04), and γ_{BC} was evaluated. γ_{BC} values were determined as the mean of three independent replicates, and the errors were determined as the SD of the mean.

Cell Cultures. Human umbilical vein endothelial cells (HUVECs) were grown in M199 medium (Gibco Life Technologies) supplemented with 20% fetal calf serum (FCS, Gibco Life Technologies), endothelial cell growth factor (100 μg/mL) (Sigma) and porcine heparin (100 μg/mL, Sigma). HUVEC were used at early passages (I−IV) and grown on plastic surface coated with porcine gelatin (Sigma). Bovine aortic endothelial cells (BAECs, provided by A. Vecchi, Istituto Clinico Humanitas IRCCS, Milan) were cultured in MEM-Eagle's medium (Gibco Life Technologies) supplemented with 10% FCS, 2% essential amino acids and 2% vitamins.

Fluorescence Resonance Energy Transfer (FRET). Vectors for the expression of the FRET pair sVEGFR2-ECFP and sVEGFR2-EYFP were obtained from Mauro Giacca (Trieste, Italy). BAECs were transiently transfected with both plasmids and seeded on NUNC multiwell chambers 48 h after transfection. After adhesion, cells were starved overnight in serum-free medium without phenol red added with 20 mM HEPES to stabilize its pH. Cells with similar expression of ECFP and EYFP proteins were stimulated with 2.0 nM gremlin, 1.2 nM VEGF-A, or vehicle. Cells were observed for 10 min before and 30 min after stimulation under the Zeiss Axiovert 200 M epifluorescence microscope equipped with a Plan-Apochromat 63x/1.4 NA oil objective. Time lapse files were analyzed by Axiovision "FRET module" software (Zeiss) using Youvan's method.[45]

Cell Proliferation Assays. Quiescent, serum-starved HUVECs treated with increasing concentrations of VEGF-A or gremlin for 24 h were added to 10 μM bromodeoxyuridine (BrdU) for 8 h. BrdU incorporation was measured with the "Cell Proliferation ELISA Biotrak System" (GE Healthcare Life Sciences) according to the manufacturer's instructions.

■ ASSOCIATED CONTENT

Supporting Information

Additional information regarding SPR raw data, CONAMORE control experiments, the relationship between nanomechanical response and extent of binding, and determination of the surface density of sVEGFR2 on the chips used for SPR and CONAMORE. This material is available free of charge via the Internet at http://pubs.acs.org.

■ AUTHOR INFORMATION

Corresponding Author

paolo.bergese@ing.unibs.it; presta@med.unibs.it

Author Contributions

‖These authors contributed equally.

Notes

The authors declare no competing financial interest.

■ ACKNOWLEDGMENTS

We thank Kimberly Hamad-Schifferli, Ivano Alessandri, and Italo Colombo. This work was supported by the Italian Ministry of Education, University and Scientific Research (grant no. PRIN2008 JWKYXB to G.O., L.E.D., and P.B.), Centro IDET and FIRB project RBAP11H2R9 2011 to M.P., AIRC (MFGA grant no. 9161 to S.M., grant no. 10396 to M.P.), FIRC (Mario-Valeria Rindi fellowship to C.R.), and CARIPLO (grant 2008-2264 and NOBEL Project to M.P.).

■ REFERENCES

(1) Alberts, B. *Cell* **1998**, *92*, 291−294.
(2) Bray, D.; Levin, M.; Morton-Firth, C. *Nature* **1998**, *393*, 85−88.
(3) Groves, J. T.; Kuriyan, J. *Nat. Struct. Mol. Biol.* **2010**, *17*, 659−665.
(4) Tomas, S.; Milanesi, L. *Nat. Chem.* **2010**, *2*, 1077−1083.
(5) Salaita, K.; Nair, P.; Petit, R.; Neve, R.; Das, D.; Gray, J.; Groves, J. *Science* **2010**, *327*, 1380−1385.
(6) Paszek, M.; Weaver, V. *Science* **2010**, *327*, 1335−6.
(7) Xu, A.; Huang, P. *Cancer Res.* **2010**, *15*, 3857−3860.
(8) Folkman, J. *Nat. Med.* **1995**, *1*, 27−31.
(9) Chung, A. S.; Lee, J.; Ferrara, N. *Nat. Rev. Cancer* **2010**, *10*, 505−514.
(10) Tvorogov, D.; Anisimov, A.; Zheng, W.; Leppanen, V.-L.; Tammela, T.; Laurinavicius, S.; Holnthoner, W.; Helotera, H.; Holopainen, T.; Jeltsch, M.; Kalkkinen, N.; Lankinen, H.; Ojala, P. M.; Alitalo, K. *Cancer Cell* **2010**, *18*, 630−640.
(11) Arlett, J.; Myers, E.; Roukes, M. *Nat. Nanotechnol.* **2011**, *6*, 203−215.
(12) Braun, T.; Backmann, N.; Vögtli, M.; Bietsch, A.; Engel, A.; Lang, H.; Gerber, C.; Hegner, M. *Biophys. J.* **2006**, *90*, 2970−2977.
(13) Federici, S.; Oliviero, G.; Hamad-Schifferli, K.; Bergese, P. *Nanoscale* **2010**, *2*, 2570−2574.
(14) Federici, S.; Oliviero, G.; Maiolo, D.; Depero, L. E.; Colombo, I.; Bergese, P. *J. Colloid Interface Sci.* **2012**, *375*, 1−11.
(15) Bergese, P.; Oliviero, G.; Colombo, I.; Depero, L. E. *Langmuir* **2009**, *25*, 4271−4273.

(16) Oliviero, G.; Maiolo, D.; Leali, D.; Federici, S.; Depero, L. E.; Presta, M.; Mitola, S.; Bergese, P. *Biosens. Bioelectron.* **2010**, *26*, 1571−1575.
(17) Fritz, J. *Analyst* **2008**, *133*, 855−863.
(18) Bergese, P.; Oliviero, G.; Alessandri, I.; Depero, L. E. *J. Colloid Interface Sci.* **2007**, *316*, 1017−1022.
(19) Ferrara, N.; Gerber, H.-P.; LeCouter, J. *Nat. Med.* **2003**, *9*, 669−76.
(20) Olsson, A. K.; Dimberg, A.; Kreuger, J.; Claesson-Welsh, L. *Nat. Rev. Mol. Cell. Biol.* **2006**, *7*, 359−371.
(21) Grunewald, F. S.; Prota, A. E.; Giese, A.; Ballmer-Hofer, K. *Biochim. Biophys. Acta* **2010**, *1804*, 567−580.
(22) Jia, H.; Bagherzadeh, A.; Bicknell, R.; Duchen, M. R.; Liu, D.; Zachary, I. *J. Biol. Chem.* **2004**, *279*, 36148−36157.
(23) Yang, Y.; Xie, P.; Opatowsky, Y.; Schlessinger, J. *Proc. Natl. Acad. Sci. U.S.A.* **2010**, *107*, 1906−1911.
(24) Ruch, C.; Skiniotis, G.; Steinmetz, M.; Walz, T.; Ballmer-Hofer, K. *Nat. Struct. Mol. Biol.* **2007**, *14*, 249−250.
(25) Mitola, S.; Ravelli, C.; Moroni, E.; Salvi, V.; Leali, D.; Ballmer-Hofer, K.; Zammataro, L.; Presta, M. *Blood* **2010**, *116*, 3677−3680.
(26) Homola, J. *Anal. Bioanal. Chem.* **2003**, *377*, 528−539.
(27) Jares-Erijman, E.; Jovin, T. M. *Nat. Biotechnol.* **2003**, *21*, 1387−1395.
(28) Rusnati, M.; Bugatti, A.; Mitola, S.; Leali, D.; Bergese, P.; Depero, L. E.; Presta, M. *Sensors* **2009**, *9*, 6471−6503.
(29) Bergese, P.; Cretich, M.; Oldani, C.; Oliviero, G.; Carlo, G.; De Depero, L. E.; Chiari, M. *Curr. Med. Chem.* **2008**, *15*, 1706−1719.
(30) For a more detailed discussion, see: Oliviero, G.; Federici, S.; Colombi, P.; Bergese, P. *J. Mol. Recognit.* **2011**, *24*, 182−187 and references cited therein.
(31) Kisko, K.; Brozzo, M. S.; Missimer, J.; Schleier, T.; Menzel, A.; Leppänen, V.-M.; Alitalo, K.; Walzthoeni, T.; Aebersold, R.; Ballmer-Hofer, K. *FASEB J.* **2011**, *25*, 2980−2986.
(32) Hall, W. P.; Modica, J.; Anker, J.; Lin, Y.; Mrksich, M.; Duyne, R. P. V. *Nano Lett.* **2011**, *11*, 1098−1105.
(33) See the original work from Young: Young, T. *Philos. Trans. R. Soc. London* **1805**, *95*, 65−87 , which has been recently digitized and is available free of charge at www.google.com/books, or in a textbook of physical chemistry, for example, ref 37.
(34) Pardali, E.; Goumans, M.-J.; ten Dijke, P. *Trends Cell Biol.* **2010**, *20*, 556−567.
(35) Grünewald, F. S.; Prota, A. E.; Giese, A.; Ballmer-Hofer, K. *Biochim. Biophys. Acta* **2010**, *1804*, 567−580.
(36) Kang, K.; Sachan, A.; Nilsen-Hamilton, M.; Shrotriya, P. *Langmuir* **2011**, *27*, 14696−14702.
(37) Adamson; Gast.*Physical Chemistry of Surfaces*; Wiley: New York, 1997.
(38) Bustamante, C.; Chemla, Y. R.; Forde, N. R.; Izhaky, D. *Annu. Rev. Biochem.* **2004**, *73*, 705−748.
(39) Ewan, L. C.; Jopling, H. M.; Jia, H.; Mittar, S.; Bagherzadeh, A.; Howell, G. J.; Walker, J. H.; Zachary, I. C.; Ponnambal, S. *Traffic* **2006**, *7*, 1270−1282.
(40) Kodadek, T. *Nat. Chem. Biol.* **2010**, *6*, 162−165.
(41) Schwille, P. *Science* **2011**, *859*, 2009−2011.
(42) Myszka, D. G. *Methods Enzymol.* **2000**, *323*, 325−332.
(43) Klotz, I. M. *Ligand-Receptor Energetics: A Guide for the Perplexed*; Wiley: New York, 2007.
(44) Karlsson, R.; Fält, A. *J. Immunol. Methods* **1997**, *200*, 121−133.
(45) Youvan, D. C.; Silva, C. M.; Bylina, E. J.; Coleman, W. J.; Dilworth, M. R.; Yang, M. M. *Biotechnology* **1997**, 1−18.